

# AttentionMixer: An Accurate and Interpretable Framework for Process Monitoring

Hao Wang *Student Member, IEEE*, Zhiyu Wang, Yunlong Niu, Zhaoran Liu, Haozhe Li, Yilin Liao, Yuxin Huang, Xinggao Liu *Member, IEEE*

**Abstract**—An accurate and explainable automatic monitoring system is critical for the safety of high efficiency energy conversion plants that operate under extreme working condition. Nonetheless, currently available data-driven monitoring systems often fall short in meeting the requirements for either high-accuracy or interpretability, which hinders their application in practice. To overcome this limitation, a data-driven approach, AttentionMixer, is proposed under a generalized message passing framework, with the goal of establishing an accurate and interpretable radiation monitoring framework for energy conversion plants. To improve the model accuracy, the first technical contribution involves the development of spatial and temporal adaptive message passing blocks, which enable the capture of spatial and temporal correlations, respectively. The two blocks are cascaded through a mixing operator. To enhance the model interpretability, the second technical contribution involves the implementation of a sparse message passing regularizer, which eliminates spurious and noisy message passing routes. The effectiveness of the AttentionMixer approach is validated through extensive evaluations on a monitoring benchmark collected from the national radiation monitoring network for nuclear power plants, resulting in enhanced monitoring accuracy and interpretability in practice.

**Impact Statement**—To meet the requirements for power conversion efficiency and carbon emissions, energy conversion plants tend to operate under increasingly extreme operating conditions to approach thermodynamic limits. Automatic monitoring of energy conversion plants is thus critical to guarantee environmental safety and energy security. Existing monitors are mainly implemented based on traditional CNN and RNN models, which are deficient in terms of accuracy and interpretability. This work pioneers a Transformer-based monitoring method, which is so far the first attempt of self-attention mechanism at both spatial and temporal scales in the context of energy conversion plant monitoring. Further, a sparsification method is devised in the training process to enhance the interpretability of the proposed model. Various experiments on a nuclear radiation monitoring down-stream task are conducted to showcase the feasibility and superiority of the proposed DAMPN. Finally, a

nationwide nuclear radiation real-time monitoring data is open-sourced on our project website<sup>1</sup>.

**Index Terms**—Artificial intelligence in energy, Time series analysis, Artificial intelligence in security, Artificial intelligence in environment.

## I. INTRODUCTION

**M**ONITORING energy conversion plants (ECPs) from high dimensional input sensory data is a critical practice to guarantee energy safety and environmental security. In recent years, as demands for power conversion efficiency and carbon emission reduction increase, ECPs tend to operate under more extreme conditions to reach the thermodynamic bound defined by the Clausius theorem. For example, in coal-based power generation plants [1], the working fluid has been operating at extremely high temperatures and pressures in recent years. Besides, in nuclear power plants, extreme operating conditions could include high temperatures and pressures of the coolant and fuel, as well as the risk of nuclear radiation leaks, which can have severe safety and environmental consequences [2], [3]. Given these extreme operating conditions, accurate and interpretable monitoring methods for must be in place to ensure the safety, security and protection of the environment.

With the advancement of measurement and learning technologies [4]–[6], data-driven approaches have been predominant for building efficient and scalable process monitors [7]–[9]. Generally, these approaches are developed in the supervised learning framework, seeking an accurate estimation of the key performance indicator (KPI) based on the historical KPI and external factors [8], [9]. Since the estimator constructed by the historical value is entirely constructed with normal logs, anomaly events can be indicated by large deviations between the actual and forecasted KPI. Therefore, this problem can be regarded as a time-series forecast task, and the identification-based methods like autoregressive (AR), moving-average (MA), and autoregressive integrated moving average (ARIMA) [10] can be employed to fulfill this task. However, the performance of these methods is greatly limited as they ignore the impact of external factors. In contrast, statistic-based methods such as the support vector regression [11] and extreme gradient boosting [12] forecast dose rates based on current external factors. These methods explicitly incorporate external factors; however, they ignore the temporal auto-correlations in data, which leads to suboptimal forecast results.

Manuscript received Sept. 28, 2022. This work is supported by the National Natural Science Foundation of China (12075212, 62073288) and Zhejiang University NGICS Platform.

Hao Wang is with the State Key Laboratory of Industrial Control Technology, Hangzhou, CO 310027 China (e-mail: haohaow@zju.edu.cn).

Zhiyu Wang is with the State Key Laboratory of Industrial Control Technology, Hangzhou, CO 310027 China (e-mail: onejoy@zju.edu.cn).

Yunlong Niu is with the State Key Laboratory of Industrial Control Technology, Hangzhou, CO 310027 China (e-mail: nyl0405@zju.edu.cn).

Zhaoran Liu is with the State Key Laboratory of Industrial Control Technology, Hangzhou, CO 310027 China (e-mail: 22032057@zju.edu.cn).

Haozhe Li is with the State Key Laboratory of Industrial Control Technology, Hangzhou, CO 310027 China (e-mail: lihaozhe@zju.edu.cn).

Yilin Liao is with the State Key Laboratory of Industrial Control Technology, Hangzhou, CO 310027 China (e-mail: liaoyl@zju.edu.cn).

Yuxin Huang is with the State Key Laboratory of Industrial Control Technology, Hangzhou, CO 310027 China (e-mail: hyx@zju.edu.cn).

Xinggao Liu is with the State Key Laboratory of Industrial Control Technology, Hangzhou, CO 310027 China (e-mail: lxg@zju.edu.cn).

This paragraph will include the Associate Editor who handled your paper.

<sup>1</sup>data.rmtc.org.cn:8080/gis/PubIndex.html

More recently, thanks to the deep learning models for their excellent capability in extracting the spatial and temporal feature automatically, process monitoring has been dominated by deep models. Various neural network models like recurrent neural network (RNN) [8], temporal convolution network (TCN) [13] and their variants [14]–[17] are gradually employed in ECP monitoring, with each owning their unique strengths and limitations. For example, RNN-based monitors can be incrementally updated for real-time monitoring, but they suffer from sub-optimal accuracy and the inference paradigm is single-threaded. Besides, these methods consist of stacked non-linear transformations, making them black boxes that cannot be interpreted. Graph neural network (GNN) depicts the relationships between arbitrary variables explicitly, rather than pills up non-linear functions that makes no physical sense, thus being prospective to improve the model accuracy interpretability. However, GNNs rely heavily on a pre-defined graph structure that is always unavailable due to the severe lack of the expert knowledge in ECPs [14].

Looking at other fields, the self-attentive mechanism [18], as a variant of GNNs that free the demand of predefined graph structure, has revolutionized performance, particularly in fundamental domains such as natural language process (NLP), computer vision (CV), and AI4Science. The architecture has domain-specific structures such as the Swin Transformer [19] for images and AlphaFold-v2 [20] for protein structures, to meet the domain-specific requirements. In the field of time series forecast,

However, in the field of ECP monitoring, the current progress stays in some direct applications of conventional network structures such as CNN and RNN. We hold the belief that the huge potential of self-attentive structures for ECP monitoring has yet to be investigated. However, two primary issues are speculated to hinder the application of self-attention for such energy conversion process monitoring under extreme working condition:

- Accuracy: where self-attention only models the temporal relationships and ignores the spatial relationships of great importance, which makes it difficult to meet the high accuracy requirement of industrial process monitors;
- Interpretability: where the dense attention matrix is filled with spurious relationships, failing to meet the high interpretability demand of industrial process monitors.

To tackle these problems, a data-driven approach named **Dual Adaptive Message Passing Network (DAMPN)** is proposed, which consists of the Spatial Adaptive Message Passing (SAMP) block, Temporal Adaptive Message Passing (TAMP) block, and Sparse Message Passing Regularisation (SMPR). Specifically, the SAMP and TAMP blocks are designed to depict the spatial and temporal relationships, respectively, which address the absence of spatial relationships to improve accuracy. Afterwards, to promise the interpretability of the proposed model, the SMPR is designed to eliminate the spurious correlations, and highlight the important relationships.

The contributions of this paper are summarized as follows:

- The first attempt of self-attention mechanism at both spatial and temporal scales in the context of energy

conversion plant monitoring.

- A sparsification method is proposed in the training process to ensure the interpretability of the proposed model under extreme working condition.
- Various experiments on a radiation monitoring downstream task are conducted to demonstrate the feasibility and superiority of the proposed DAMPN.

The remaining sections are structured as follows: Section II introduces the preliminaries to better understand the proposed DAMPN. Section III describes the architecture and learning objective of DAMPN. To demonstrate its superiority application to extreme working condition energy conversion plant, a real industrial case study on the nuclear radiation monitoring is conducted in Section IV. Conclusions and future works are discussed in Section V.

## II. PRELIMINARIES

### A. Message Passing Mechanism

The message passing mechanism is a generalized GNN framework, and many space-based GNN models, such as GCN, GraphSAGE, and GAT, can be considered as a special case of the message passing mechanism [21]. Let  $\mathcal{M}$  and  $\mathcal{U}$  be the message generation function and state update function, respectively; the  $k$ -th round of message passing for node  $\nu_i$  can be expressed as follow:

$$\begin{aligned} m_i^k &= \sum_{\nu_j \in \mathbb{N}_{\mathcal{G}}(\nu_i)} \mathcal{M}(F_i^k, F_j^k), \\ F_i^{k+1} &= \mathcal{U}(m_i^k, F_i^k), \end{aligned} \quad (1)$$

where  $F_i^k$  is the feature embedding of node  $\nu_i$ . In (1), the message function  $\mathcal{M}$  generates the message features from the neighbors (whose set is denoted as  $\mathbb{N}$ ) of node  $\nu_i$ , and the update function  $\mathcal{U}$  bounds for updating the features of node  $\nu_i$  by fusing the message features  $m_i^k$  and the original features  $F_i^k$ . However, the message passing mechanism cannot be directly used in complex industrial process monitoring as it requires a predefined graph which defines the neighbors of  $\nu_i$  explicitly.

### B. Self-attention Mechanism

Let  $\mathbf{Q} \in \mathbb{R}^{T \times D}$ ,  $\mathbf{K} \in \mathbb{R}^{T \times D}$ , and  $\mathbf{V} \in \mathbb{R}^{T \times D}$  be the query, key, and value space, respectively; the celebrated self-attention mechanism [18] can be expressed as follow:

$$\mathbf{H} = \text{SoftMax}\left(\frac{\mathbf{Q}\mathbf{K}^T}{\sqrt{D}}\right)\mathbf{V}, \quad (2)$$

where  $\mathbf{H} \in \mathbb{R}^{T \times D}$  can be regarded as an aggregated message feature in the value space according to the similarity between arbitrary nodes. As such, (2) can be treated as a special kind of message passing mechanism defined in (1), while it does not rely on a predefined graph, which indicates that it can be regarded as a key to solve the monitoring problem for complex process without any prior knowledge.

### C. Graph Structure Sparsification

The adaptive generated graph structure using (1) is always highly dense [22], which hinders the models' interpretability, and thus the application in monitoring energy conversion plants under extreme working condition. Moreover, according to Occam's razor principle, meaningful relationships in the physical world are always sparse, which implies that there are spurious relationships in the learned (dense) graph structure, and thus the risk of overfitting. To these ends, researchers have turned to explore graph sparsification techniques [23] to learn interpretable and meaningful graph structures. Intuitively, sampling is a natural choice, *e.g.*, MTGNN [24] which samples the top- $k$  elements in the graph matrix. As an extended Transformer model, Informer [25] proposed a score function, which is an approximation of the KL divergence between the graph distribution and uniform distribution. Although existing works have had great success in obtaining sparse graph structures, most of them rely on sampling techniques and thus suffer from significant variance in both training and inference phases, which is unacceptable in process monitoring under extreme working conditions.

## III. METHODOLOGY

This section proposes the Dual Adaptive Message Passing Network for accurate and interpretable industrial process monitoring under extreme working conditions. It is built upon the message passing framework in Section II for modeling relationships between variables. Based on the framework, a Spatial Adaptive Message Passing (SAMP) block and Temporal Adaptive Message Passing (TAMP) block are proposed in Section III-B and III-C, respectively, to depict the spatio-temporal relationships and improve accuracy. A Sparse Message Passing Regularisation (SMPR) is further proposed in Section III-D, which is an efficient sparsification strategy that eliminates spurious relationships without sampling procedure. The overall architecture and learning objective are summarized in Section III-E.

### A. Problem Definition

In this paper, bold uppercase letters, *e.g.*,  $\mathbf{X}$  denote matrix, and lowercase letters, *e.g.*,  $\mathbf{x}$  denote associated vectors. Let  $\mathbf{x}_t \in \mathbb{R}^D$  be the observation at time step  $t$ , where  $D$  is the number of features (*i.e.*, the spectral measures, the meteorological conditions, and spectrometer operating conditions). Given historical observations  $\mathbf{X}_t := [\mathbf{x}_{t+1}, \mathbf{x}_{t+2}, \dots, \mathbf{x}_{t+T}]$  with window size  $T$ , the problem aims to learn a function  $f: \mathbb{R}^{T \times D} \rightarrow \mathbb{R}$  such that  $f(\mathbf{X}_t) \rightarrow y_t^H$ , where  $y_t^H$  is the actual dose rate at the  $t + T + H$  step.

### B. Spatial Adaptive Message Passing Module

SAMP module adapts the self-attention network [18] to free the demand for pre-defined graphs. Existing vanilla self-attention [18] generate messages for each time steps and aggregate messages through the similarity between time steps. This approach ignores the spatial relationships between observed variables and thus get sub-optimal accuracy. SAMP module

models spatial relationships between variables to fill the gap and improve the accuracy. Fig. 1 (b) depicts the  $k$ -th round of spatial message passing, with input  $\mathbf{S}^{k,\text{in}} \in \mathbb{R}^{D \times T}$  and output  $\mathbf{S}^{k,\text{out}} \in \mathbb{R}^{D \times T}$ , where  $T$  is the sequence length,  $D$  is the hidden dimension. It consists of three steps as follows.

1) *Message Generation*: The message embedding  $\mathbf{V}_S^k \in \mathbb{R}^{D \times T}$  is obtained by feeding the state embeddings into a Multilayer Perceptron (MLP) layer:

$$\mathbf{V}_S^k := \text{MLP}(\mathbf{S}^{k,\text{in}}), \quad (3)$$

where  $\mathbf{V}_S^k [i] \in \mathbb{R}^T$  is the message embedding of the  $i$ -th node, the MLP layer consists of a learnable affine transformation followed by a Rectified Linear Unit (ReLU) [26].

2) *Message Aggregation*: Each node generates its update embedding by aggregating its neighboring message embeddings. First, the strength matrix of message passing  $\mathbf{M}_S^k \in \mathbb{R}^{D \times D}$  between arbitrary nodes is defined as

$$\begin{aligned} \mathbf{Q}_S^k &:= \text{MLP}(\mathbf{S}^{k,\text{in}}), \\ \mathbf{K}_S^k &:= \text{MLP}(\mathbf{S}^{k,\text{in}}), \\ \hat{\mathbf{M}}_S^k &:= \mathbf{Q}_S^k * [\mathbf{K}_S^k]^T / \sqrt{D}, \\ \mathbf{M}_S^k &:= \text{SoftMax}(\hat{\mathbf{M}}_S^k), \end{aligned} \quad (4)$$

where  $\mathbf{M}_S^k [i, j]$  is a generalized similarity measure between the  $i$ -th node and the  $j$ -th node; the division of  $\sqrt{D}$  avoids numerical errors during optimization [18]; the SoftMax operation is utilized to normalize the message passing strength:

$$\mathbf{M}_S^k [i, j] := \frac{\exp(\hat{\mathbf{M}}_S^k [i, j])}{\sum_{i=1}^D \exp(\hat{\mathbf{M}}_S^k [i, j])}. \quad (5)$$

Noting that

- $\mathbf{M}_S^k$  is adaptively generated from data, thus escaping the message passing's demand for a pre-defined graph;
- $\mathbf{M}_S^k$ 's excessive density hinders its accuracy and interpretability, inspiring the regularizer in Section III-D;
- $\mathbf{M}_S^k$  is asymmetric, *i.e.*,  $\mathbf{M}_S^k [i, j] \neq \mathbf{M}_S^k [j, i]$  because  $\mathbf{Q}_S^k \neq \mathbf{V}_S^k$ , bringing better monitoring performance as detailed in Section IV-D.

A plain intuition is that neighbors with more remarkable similarities always convey more important messages. As such, the update embeddings  $\mathbf{U}_S^k \in \mathbb{R}^{D \times T}$  is calculated as

$$\mathbf{U}_S^k := \mathbf{M}_S^k * \mathbf{V}_S^k, \quad (6)$$

where the  $i$ -th node's update embedding is a weighted sum of the message embeddings of its neighbours, with the weight being its similarity to its neighbours:

$$\mathbf{U}_S^k [i, :] := \sum_{j=1}^D \mathbf{M}_S^k [i, j] \mathbf{V}_S^k [j, :]. \quad (7)$$

3) *State Update*: State embeddings are renewed with previous state embeddings  $\mathbf{S}^{k,\text{in}}$  and update embeddings  $\mathbf{U}_S^k$ :

$$\mathbf{S}^{k,\text{out}} := \text{LayerNorm}(\mathbf{S}^{k,\text{in}} + \mathbf{U}_S^k), \quad (8)$$

where the residual link preserves the previous state embeddings that is excluded in the generation process of  $\mathbf{U}_S^k$ ; the layer normalization (LayerNorm) standardizes the data distribution at each time step to stabilize the training process.

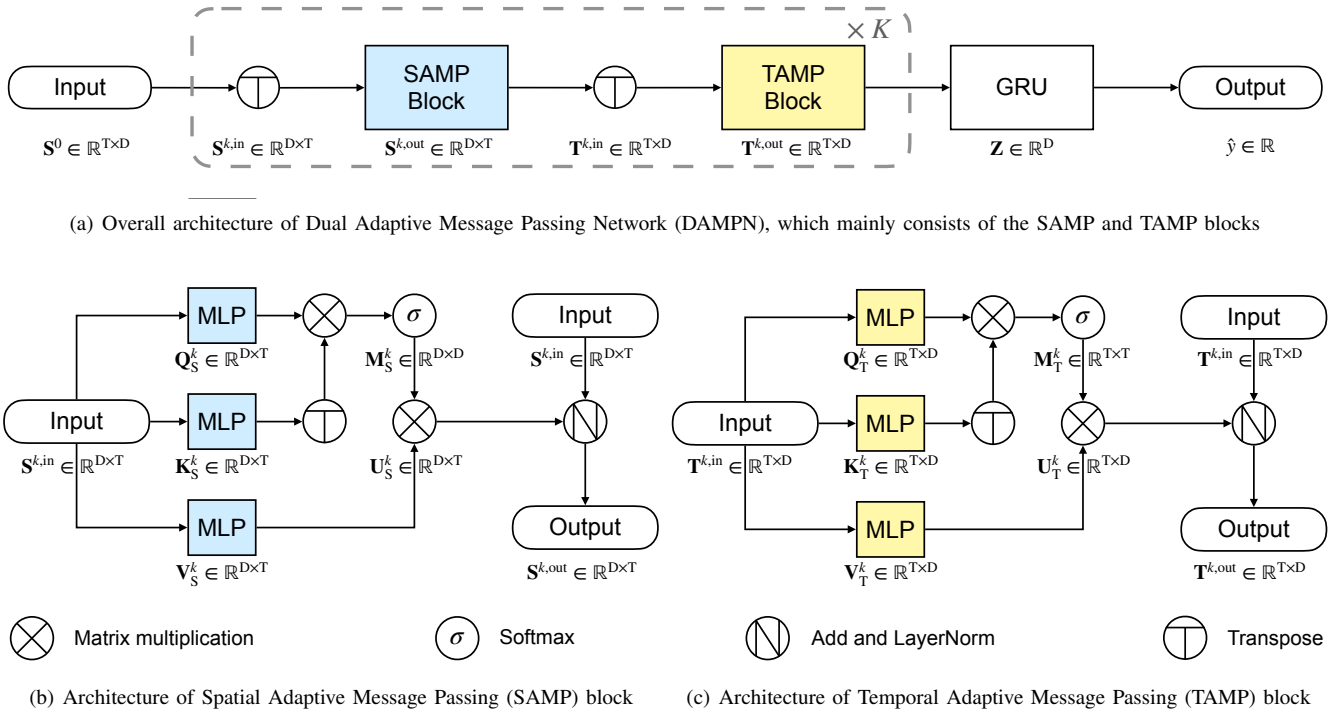


Fig. 1. The architecture of proposed model, where each module's output is marked under the corresponding module.

### C. Temporal Adaptive Message Passing Module

SAMP focuses on the spatial relationships while ignores the temporal relationships, making the TAMP module essential. The  $k$ -th round of temporal message passing is shown in Fig. 1 (c) with input  $\mathbf{T}^{k,in} \in \mathbb{R}^{T \times D}$  and output  $\mathbf{T}^{k,out} \in \mathbb{R}^{T \times D}$ . Different from SAMP, TAMP models the temporal relationship between time steps, which views the input  $\mathbf{T}^{k,in}$  as the state embeddings of T nodes, and describes the temporal similarity with  $\mathbf{M}_T^k \in \mathbb{R}^{T \times T}$ . As the structure and intuition are largely similar to SAMP, a detailed description is omitted for brevity.

### D. Sparse Message Passing Regularizer

As shown in Fig. 6 (a), the relationships learned by DAMPN are dense, while the actual relationships in the physical world are sparse [27], [28] according to Occam's razor principle. It means that there exist many spurious relationships, which leads to the risk of overfitting and obscures meaningful relationships [29], thus harming the accuracy and interpretability of DAMPN. Therefore, mining sparse graph structure is critical for building interpretable and reliable process monitors.

Existing approaches [24], [25] mainly achieve graph sparsification with sampling methods, which may be complex and unstable for real-time process monitoring application. To this end, instead of introducing the sampling process in the model inference, regularization on the graph (self-attention matrix) during the training process would be a better choice. Since the message passing over the graph can be treated as a special kind of ordinary/partial differential equation, previous strategy in the context of nonlinear dynamical system sparse identification

[28], [30] can be adopted:

$$\mathcal{L}_{\text{smp}} := \sum_{k=1}^K \|\mathbf{M}_S^k\|_F + \sum_{k=1}^K \|\mathbf{M}_T^k\|_F, \quad (9)$$

where the  $\|\cdot\|_F$  indicates the Frobenius norm, which can encourage the sparse solution during the model training process. Throughout the Frobenius norm in the loss function, the  $\mathbf{M}_S^k$  and  $\mathbf{M}_T^k$ , highlights meaningful relationships without sampling on the graph matrix, and thus improves DAMPN's accuracy and interpretability.

### E. Dual Adaptive Message Passing Network

1) *Overall Architecture*: As shown in Fig. 1 (a), DAMPN mainly consists of cascaded SAMP and TAMP blocks. Specifically, the preprocessed data is first fed into SAMP, *i.e.*,  $\mathbf{S}^{1,in} = \mathbf{S}^0$ , where messages are passed through the adaptive spatial graph. Then, the spatial and temporal dimensions of SAMP's output are transposed to obtain the input to TAMP:

$$\begin{aligned} \mathbf{S}^{k,out} &:= \text{SAMP}(\mathbf{S}^{k,in}), \\ \mathbf{T}^{k,in} &:= \text{Transpose}(\mathbf{S}^{k,out}), \end{aligned} \quad (10)$$

where  $k \leq K$  is the round of current message passing. Afterwards, TAMP extracts the temporal relationships in the data, and the transpose of its output is the input to SAMP block in the next round of message passing:

$$\begin{aligned} \mathbf{T}^{k,out} &:= \text{TAMP}(\mathbf{T}^{k,in}), \\ \mathbf{S}^{k+1,in} &:= \text{Transpose}(\mathbf{T}^{k,out}). \end{aligned} \quad (11)$$

Finally, the information of  $K$ -th TAMP's output is aggregated via a GRU block to get the dose rate estimate:

$$\mathbf{Z} := \text{GRU}(\mathbf{T}^{K,out}), \quad \hat{y}_t^H := \text{Linear}(\mathbf{Z}), \quad (12)$$

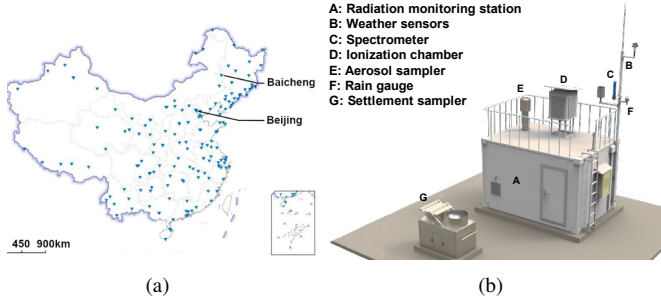


Fig. 2. National automatic nuclear radiation monitoring network in China: (a) distribution of established monitoring stations; (b) schematic diagram of each monitoring station.

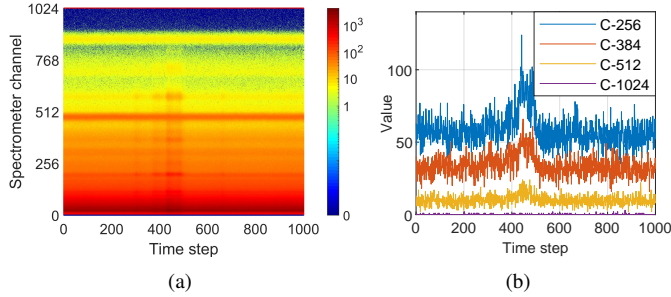


Fig. 3. Spectrometer measurements and dose rates of 1000 sequential time steps starting from 2020/5/15 21:54:00, in Baicheng Station, Jilin.

where  $\hat{y}_t^H$  is DAMPN’s output,  $H$  is the forecasting horizon,  $\text{Linear}(\cdot)$  is a MLP-layer without nonlinear transformation.

2) *Learning Objective*: The learning objective aims to minimize the error of forecast and the density of message passing. Given input  $\mathbf{X}_t$  and label  $y_t^H$ , the forecast error is

$$\mathcal{L}_{\text{pred}} := (y_t^H - \hat{y}_t^H)^2, \quad (13)$$

where  $y_t^H$  is the actual radiation dose rate at the  $t + H$  time step,  $\hat{y}_t^H$  is the output of the proposed DAMPN given input  $\mathbf{S}^0 := \mathbf{X}_t$ . The overall learning objective is

$$\mathcal{L}_{\text{DAMPN}} = \mathcal{L}_{\text{pred}} + \lambda \cdot \mathcal{L}_{\text{smpr}}, \quad (14)$$

where  $\lambda$  controls the strength of SMPR. The network structure and learning objective cooperate to improve accuracy and interpretability, both critical for nuclear radiation monitoring.

#### IV. EXPERIMENTS

To demonstrate the effectiveness of the proposed DAMPN model for extreme working condition energy conversion process, experiments are conducted on the nuclear radiation monitoring downstream task with monitoring data from industrial nuclear power plants.

##### A. Background of Nuclear Radiation Monitoring

As a resilient and reliable source of energy [31], [32], nuclear power plants generate nearly 800 billion kilowatt-hours of electricity per year in America, supplying more than 60% of the emission-free electricity, reducing about 500 million metric tons of carbon emission [33]. However,

TABLE I  
VARIABLE DEFINITION FOR THE MONITORING DATA

Field	Unit of measure
<b>Atmospheric radiation</b>	
Dose rate	nGy / h
Spectrum (1024 channels)	ANSI/IEEE N42.42
<b>Meteorological conditions</b>	
Temperature	°C
Humidity	%
Atmosphere pressure	hPa
Wind direction	Clockwise angle
Wind speed	m / s
Precipitation indicator	Boolean value
Amount of precipitation	mm
<b>Spectrometer operating conditions</b>	
Battery voltage	V
Spectrometer voltage	V
Spectrometer temperature	°C

since the nuclear power plants mainly operate under extreme working conditions, their potential for environmental safety and energy security raises intense concerns [2], [3]. In nuclear anomalies, excessive amounts of radionuclides would be released into the atmosphere, causing severe environmental pollution. As a preventive technology, automatic monitoring networks for nuclear power plants have been widely deployed, *e.g.*, the RadNet of the Environmental Protection Agency in America [34] and the Fixed Point Surveillance network of the Radiation Protection Bureau in Canada [35]. As shown in Fig. 2, there have been around 500 monitoring stations for nuclear radiation in the Chinese Atmospheric Nuclear Radiation Monitoring Network.

The monitoring objective is  $\gamma$ -ray dose rate in the atmosphere [36], which reflects the intensity of most radionuclides. Adding to the challenge is that the measured dose rate is not only related to radionuclide emissions but also affected by meteorological conditions and spectrometer operating conditions [37], [38]. For example, the natural radionuclide radon in the air would be washed to the ground during rainfall, leading to a spurious increase of the dose rate measured by monitoring sensors [37]. Ignoring such external factors can lead to false alarms and consequently reduce the reliability of monitoring.

To this end, the data collected include atmospheric radiation data, meteorological conditions, and spectrometer operating conditions in Table I. For atmospheric radiation data, two sensors, *i.e.*, the ionization chamber and the spectrometer, are employed in each station. The ionization chamber measures  $\gamma$ -ray dose rate [39], and its measurements are uploaded daily on our online monitoring board<sup>2</sup>. The spectrometer<sup>3</sup> measures spectrum, an essential indicator of radionuclide concentrations in the industrial environment. Fig. 3 (a) shows a 1024-channel spectrum where different channels show different patterns of variation, with the energy decaying in higher channels. Fig. 3 (b) details the dynamics in spectrums with four selected channels, which are non-stationary and noise-filled due to the disturbance of external factors. To calibrate such external

<sup>2</sup>Real-time dose rate data has been released on [our website](#).

<sup>3</sup>The spectrometer employs the SARA detector by ENVINET GmbH.

TABLE II  
DESCRIPTION OF SAMPLING STRATEGY.

Station	Location	#Sample	#Variable	Interval	Start time
Changchi	Beijing	38,686	1,034	5 min	10/3/2020
Industrial Park	Jilin	38,687	1,034	5 min	21/4/2020

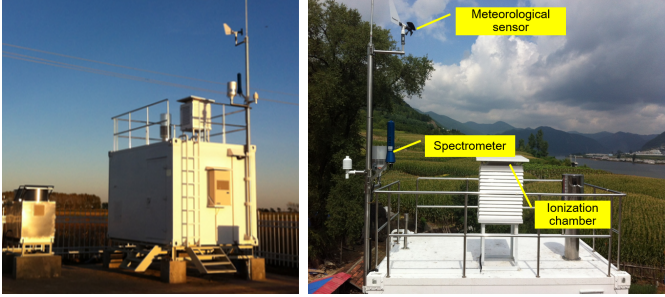


Fig. 4. Nuclear monitoring stations with data collection components.

impacts, the meteorological conditions, *e.g.*, precipitation, and spectrometer operating conditions, *e.g.*, battery voltage, are supplemented to improve the accuracy of radiation monitoring.

### B. Experimental Setup

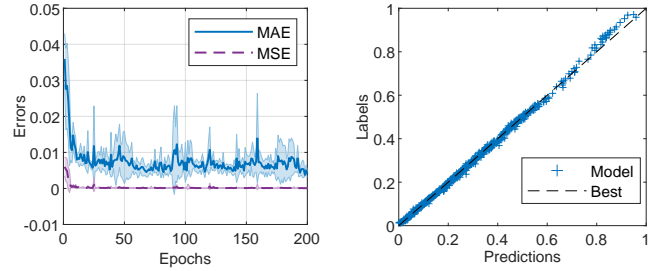
1) *Datasets*: Two industrial benchmarks are constructed based on the observations from the national radiation monitoring network, one monitor of which is shown in Fig. 4. The 1034 input variables are described in Table I, including the 1024-channel spectrum, 7-channel meteorological conditions, and 3-channel spectrometer operating conditions. Table II complements the sampling strategy to construct both benchmarks in practice. Both benchmarks are divided for training, validation, and test in chronological order in the ratio 0.7:0.15:0.15 and scaled with a min-max scaler.

2) *Baselines*: DAMPN is compared with three groups of baselines. (1) Identification-based models: Auto-Regression (AR) [10], Moving Average (MA) [10], AutoRegressive Integrated Moving Average (ARIMA) [10]; (2) Statistic-based models: Lasso Regression (LASSO) [40], Support Vector Regression (SVR) [11], Random Forest (RF) [41], Gradient Boosting Decision Tree (GBDT) [12], eXtreme Gradient Boosting (XGB) [12]; (3) Deep models: Long Short-Term Memory (LSTM) [42], Gated Recurrent Unit (GRU) [43].

3) *Training Strategy*: All deep models are trained for 200 epochs using Adam [44] optimizer. The dropout rate is 0.1, the batch size is 64, the window size is  $T = 16$ , the learning rate is 0.001 with a cyclic schedule, and the round of message passing is  $K = 2$ . This setup is applied to all methods to make them convergent and comparison fair. The strength of SMPR is  $\lambda = 0.03$  according to Section ?? . Each model is check-pointed on the validation set every epoch, and the best model's performance on the test set is reported.

4) *Evaluation Strategy*: The Coefficient of Determination ( $R^2$ ) is used as the main fitness metric in line with [14], [16].

$$R^2 = 1 - \frac{\sum_{t=1}^N (y_t^H - \hat{y}_t^H)^2}{\sum_{i=1}^N (y_i^H - \bar{y}_i^H)^2}, \quad (15)$$



(a) Forecast error on training set (b) Forecast accuracy on test set

Fig. 5. Visualization of DAMPN performance on Baicheng benchmark, with the dashed line being the mean value and the corresponding shaded area being the 95% confidence interval.

where  $y_t^H$  is the actual dose rate,  $\hat{y}_t^H$  is the estimated dose rate,  $\bar{y}_t^H$  is the mean value of  $y_t^H$  for  $t = 1 : N$ ,  $N$  is the size of test set. To better quantify the estimation error of each model, Mean Squared Error (MSE) and Mean Absolute Error (MAE) are employed as additional metrics:

$$\begin{aligned} \text{MSE} &= \frac{1}{N} \sum_{t=1}^N (y_t^H - \hat{y}_t^H)^2, \\ \text{MAE} &= \frac{1}{N} \sum_{t=1}^N |y_t^H - \hat{y}_t^H|. \end{aligned} \quad (16)$$

### C. Performance comparison

The performance of DAMPN and its competitors are compared in Table III under four forecast horizons  $H = 1, 3, 5, 7$ , and the observations are summarized as follows.

Identification-based models conduct practical short-term forecasts on both benchmarks. For example, ARIMA achieves a  $R^2$  of 0.77 and 0.79 on the Beijing and Baicheng benchmarks, respectively, which validates the autocorrelation characteristics of both benchmarks. However, they can only describe linear autocorrelation, leaving long-term forecast performance vulnerable to the non-linear autocorrelation in datasets. In particular, for  $H=7$ , ARIMA achieves a  $R^2$  of 0.73 on the Beijing benchmark but merely 0.12 on the Baicheng benchmark. This dramatic drop is attributed to the strong non-linear autocorrelation in the Baicheng benchmark.

Statistic-based models incorporate external factors such as meteorological and spectral measures, showing competitive short-term forecast performance. In particular, non-linear estimators (RF, GBDF, XGB) with larger capacity outperform linear estimators (LASSO, SVR). For example, the MAE of RF on the two benchmarks is 0.033 and 0.0159, respectively, both significantly higher than that of LASSO and SVR. A drawback is that the performance decays as the forecast horizon increases, as they ignore the temporal autocorrelation in data. For example, the  $R^2$  of XGB drops from 0.894 at  $H=1$  to 0.7684 at  $H=5$  and 0.671 at  $H=7$  on the Beijing benchmark.

Deep models capture both externalities and autocorrelation, thus achieving the best short-term forecast performance among all baselines. In addition, they depict the non-linear autocorrelation in data, making the performance less vulnerable to the

TABLE III  
COMPARATIVE STUDY ON THE BEIJING AND BAICHENG BENCHMARKS OVER FOUR FORECAST HORIZONS.

Methods	Metrics	Beijing Station				Baicheng Station				
		H=1	H=3	H=5	H=7	H=1	H=3	H=5	H=7	
Identification based models	AR	MAE	0.0925	0.1005	0.1068	0.1161	0.0999	0.1329	0.1669	0.1899
		R <sup>2</sup>	0.7672	0.7265	0.6887	0.6455	0.7051	0.5110	0.2196	-0.0282
	MA	MAE	0.0952	0.1027	0.1081	0.1161	0.1537	0.1794	0.2019	0.2201
		R <sup>2</sup>	0.7563	0.7193	0.6828	0.6437	0.3457	0.1095	-0.1363	-0.3642
	ARIMA	MAE	0.0962	0.0982	0.1048	0.1000	0.0818	0.1094	0.1452	0.1762
		R <sup>2</sup>	0.7700	0.7339	0.7228	0.7342	0.7954	0.6611	0.3940	0.1258
Statistic based models	LASSO	MAE	0.0500	0.0511	0.0527	0.0546	0.0207	0.0210	0.0216	0.0224
		R <sup>2</sup>	0.4015	0.3663	0.3124	0.2491	0.3998	0.3708	0.3260	0.2719
	SVR	MAE	0.0723	0.0712	0.0677	0.0664	0.0486	0.0599	0.0647	0.0655
		R <sup>2</sup>	0.4743	0.4843	0.4828	0.4429	0.3247	-0.0073	-0.2074	-0.2936
	RF	MAE	0.0337	0.0360	0.0383	0.0413	0.0159	0.0171	0.0172	1.0183
		R <sup>2</sup>	0.8580	0.8193	0.7589	0.6753	0.8918	0.8393	0.7879	0.7118
	GBDT	MAE	0.0396	0.0406	0.0420	0.0444	0.0176	0.0175	0.0178	0.0183
		R <sup>2</sup>	0.7453	0.7137	0.6543	0.5678	0.7840	0.7559	0.7057	0.6460
	XGB	MAE	0.0302	0.0332	0.0370	0.0412	0.0105	0.0118	0.0136	0.0149
		R <sup>2</sup>	0.8943	0.8393	0.7684	0.6719	0.9485	0.9012	0.8335	0.7555
Deep models	LSTM	MAE	0.0070*	0.0084	0.0101	0.0089*	0.0098*	0.0122*	0.0136	0.0121*
		R <sup>2</sup>	0.9721*	0.9710	0.9628	0.9697*	0.9755*	0.9646*	0.9588	0.9677*
	GRU	MAE	0.0101	<b>0.0071*</b>	<b>0.0083*</b>	0.0097	0.0134	0.0127	0.0084*	0.0158
		R <sup>2</sup>	0.9691	0.9712*	0.9730*	0.9123	0.9598	0.9631	0.9626*	0.9494
Current work	DAMPN	MAE	<b>0.0034</b>	0.0127	0.0102	<b>0.0085</b>	<b>0.0029</b>	<b>0.0048</b>	<b>0.0049</b>	<b>0.0114</b>
		R <sup>2</sup>	<b>0.9957</b>	<b>0.9861</b>	<b>0.9806</b>	<b>0.9763</b>	<b>0.9938</b>	<b>0.9858</b>	<b>0.9803</b>	<b>0.9803</b>

\* marks the best baseline for each metric; bolded results indicate the best method for each metric.

TABLE IV  
ABLATION STUDY ON THE BAICHENG BENCHMARK

Variants	MSE	MAE	R <sup>2</sup>
w/o SAMP	0.0009±0.0001 <sup>†</sup>	0.0146±0.0007 <sup>†</sup>	0.8691±0.0813 <sup>†</sup>
w/o TAMP	0.0001±0.0000	0.0041±0.0006 <sup>†</sup>	0.9923±0.0045 <sup>†</sup>
w/o SMPR	0.0001±0.0000	0.0044±0.0042	0.9857±0.2438
w/o direction	0.0001±0.0000	0.0048±0.0035	0.9877±0.2768
DAMPN	<b>0.0001±0.0000</b>	<b>0.0034±0.0005</b>	<b>0.9957±0.0032</b>

<sup>†</sup> marks the variants that DAMPN outperforms significantly at p-value < 0.05 over paired samples t-test. Bolded results indicate the best in each metric.

TABLE V  
COMPLEXITY ANALYSIS OF FOUR BLOCKS

Blocks	Complexity	Sequential Ops	Path Length
RNN	$\mathcal{O}(T \cdot D^2)$	$\mathcal{O}(T)$	$\mathcal{O}(T)$
TCN	$\mathcal{O}(\tau \cdot T \cdot D^2)$	$\mathcal{O}(1)$	$\mathcal{O}(\log_{\tau} T)$
TAMP	$\mathcal{O}(T^2 \cdot D)$	$\mathcal{O}(1)$	$\mathcal{O}(1)$
SAMP	$\mathcal{O}(T \cdot D^2)$	$\mathcal{O}(1)$	$\mathcal{O}(1)$

forecast horizon. For example, on the Baicheng benchmark, the R<sup>2</sup> of GRU drops a mere 0.01 from H=1 to H=7, around 5% of XGB's and 2% of ARIMA's performance drop.

DAMPN further improves the monitoring accuracy based on deep models. For example, it improves the R<sup>2</sup> of GRU by 2.74%, 1.53%, 0.78%, and 7.01%, respectively, on the Beijing benchmark at four horizons. Combined with the aforementioned comparisons, its superior performance is attributed to the adaptive message passing mechanism, explicitly depicting the non-linear spatial and temporal relationships. Fig. 5 details DAMPN's performance<sup>4</sup>. In the training phase, it converges rapidly, as evidenced by the loss function MSE reaching around zero within five epochs. In the test phase, it estimates the dose rates accurately, as shown by the distribution of estimated and actual values around a line with a slope of 1.

#### D. Ablation Study

Accuracy is the first critical requirement for monitoring energy conversion plants under extreme working conditions.

<sup>4</sup>The forecast error should be non-negative according to (16). The shaded area in Fig. 5 contains several negative values, which is reasonable because it indicates confidence interval rather than the exact performance in practice.

To further evaluate the effectiveness of DAMPN's components in improving accuracy, four variants of DAMPN in Table IV are designed as follows:

- 1) w/o SAMP: DAMPN without the SAMP module;
- 2) w/o TAMP: DAMPN without the TAMP module;
- 3) w/o SMPR: DAMPN without the SAMP, *i.e.*, set  $\lambda = 0$ ;
- 4) w/o direction: DAMPN with undirected message passing graph, *i.e.*,  $\mathbf{Q}_S^k = \mathbf{K}_S^k$  and  $\mathbf{Q}_T^k = \mathbf{K}_T^k$  for  $k = 1, \dots, K$ .

SAMP improves R<sup>2</sup> from 0.869 to 0.995, significantly passing the two-sample t-test. This improvement is attributed to the fact that SAMP addresses the absence of spatial relations in vanilla self-attentions, backing up the claim in Section III-B.

TAMP reduces MAE from 0.0041 to 0.0034, which also passes the two-sample t-test. It comes from the explicit description of temporal relationships, validating Section III-C.

Removing SMPR from DAMPN leads to decreased forecast accuracy because the message passing matrices learned without SMPR are dense, as shown in Fig. 6. It brings a potential risk of overfitting and thus hinders DAMPN's generalization. This performance drop verifies the claims in Section III-D.

The undirected message passing graph hinders monitoring performance, with R<sup>2</sup> from 0.995 to 0.987, as it fails to model the asymmetric relationships in data. Temporally, the node of a later moment is always the consequence of the

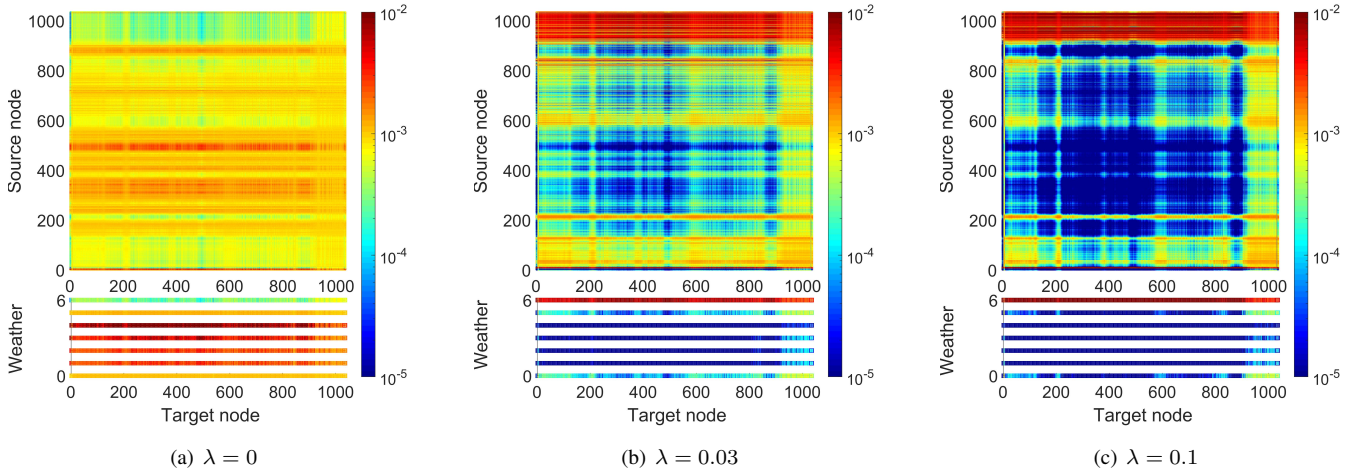


Fig. 6. Visualization of spatial graphs in the first SAMP module with different strengths of sparse message passing regularization  $\lambda$ .

node of an earlier moment, and the reverse does not hold. Spatially, meteorological conditions are always responsible for dose-rate measures, and the reverse is false. For example, in Fig. 6 (b-c), links from precipitation (the 6-th source variable) to spectrometer measurements are significantly potent than the corresponding inverse links. Therefore, asymmetry is definitely present in nuclear radiation monitoring logs, and ignoring this property reduces model accuracy.

### E. Interpretability Case Study

Interpretability is the second requirement for monitoring energy conversion plants. Fig. 6 visualizes the spatial message passing strengths  $M_S^{k=1}$ , which demonstrates that DAMPN improves interpretability from the three aspects as follows.

First, most deep models such as RNNs and TCNs consist of stacked non-linear transformations without any physical sense. Existing self-attention methods make predictions based on the relationships between time steps, making it feasible to identify the autoregressive relationships in data. However, they fail to depict the spatial relationship between variables, which is a more concerned topic for ECP monitoring task. To address this issue, SAMP provides an explicit and transparent modeling of spatial correlations which makes it feasible to visualize the attention weights for different input variables when making decision.

Second, as shown in Fig. 6 (a), the message passing without SMPR is highly dense. However, the actual relationships in the physical world are sparse [29], [45]. This implies the existence of many spurious relations that obscure meaningful spatial relations and impair interpretability. As the strength of the SMPR increases, message passing is gradually sparsified and spurious relationships are eliminated, as shown in the dark red part of Fig. 6 (b-c). As a result, the meaningful relationships are highlighted and model interpretability is improved, which backs up our claims in Section III-D.

Third, the reliability of DAMPN's interpretation is further validated by its consistency with existing expert knowledge. Specifically, the lower half of Fig. 6 details the impact of

weather conditions on other measurements, where the sixth weather condition (precipitation) is highly correlated with most spectrometer measures, highlighted by SMPR. This correlation between precipitation and spectrometer measures holds mechanically, since radionuclide radon in the air would be washed to the ground during rainfall, leading to a spurious increase of spectrometer measures [36], [37].

### F. Complexity Analysis Study

Table V reports computational costs following [18], where methods are employed to transform one sequence  $(\mathbf{x}_1, \dots, \mathbf{x}_T)$  to another sequence  $(\mathbf{z}_1, \dots, \mathbf{z}_T)$  with equal length  $T$  and hidden dimension  $D$ . Three metrics are considered as follows:

- Complexity: the amount of floating-point operations, which is the primary measure of computational cost;
- Sequential Ops: the number of operations that cannot be parallelized, which hinders the GPU acceleration;
- Path Length: the minimum number of layers to model the relationships between any time steps, which measures the model's efficiency for long-term dependencies.

For RNNs, the sequential operations and path length lead to inefficiencies in training and inference. For TCNs with kernel length  $\tau$ , all computations can be parallelized; however, the path length leads to the need to cascade many TCN layers to build global relationships and thus hinders efficiency for long-term dependencies. For TAMPs, *i.e.*, the vanilla self-attention block, the superiority includes parallelization and path length, while the complexity  $\mathcal{O}(T^2)$  leaves it difficult to handle long input signals [29], [45].

The proposed SAMP enjoys the superiority of parallelization and path length, and reduces the complexity *w.r.t.* sequence length to  $\mathcal{O}(T)$ . A potential drawback is its second-order complexity for hidden dimensions  $D$ , which can be mitigated by mapping the input data into a smaller hidden dimension before the SAMP block.

## V. CONCLUSION

To meet the requirement on accuracy and interpretability for monitoring energy conversion process under extreme



working condition, this paper depicts the spatial and temporal relationships with a generalized self-attention architecture, and devised a data-driven approach named DAMPN. In the DAMPN, the self-attention was designed at a spatial and temporal scale to enable the model extract spatio-temporal features from data as far as possible. Besides, to promise the interpretability of the learnt graph, a regularization term was designed in the loss function innovated by sparse identification of nonlinear dynamical system. Furthermore, to demonstrate the superiority of the proposed DAMPN, a downstream task on the radiation monitoring for nuclear plant was proposed. The comparison experiment demonstrated the superiority of the proposed model. Ablation study explained the reason for the superiority. Finally, an explainable experiment was conducted to illustrate the interpretability of the proposed DAMPN.

There are two directions of future work that we intend to pursue. The first direction seeks to encode existing expert knowledge into sparse attentions [29], [45] to further enhance the accuracy and interpretability. The second direction attempts to deploy the proposed model onto our online monitoring board<sup>1</sup> to serve nuclear power plants nationwide.

## REFERENCES

- [1] X. Wu, X.-H. Xia, G. Chen, X. Wu, and B. Chen, "Embodied energy analysis for coal-based power generation system-highlighting the role of indirect energy cost," *Appl. Energy*, vol. 184, pp. 936–950, 2016.
- [2] F.-C. Chen and M. R. Jahanshahi, "Nb-cnn: Deep learning-based crack detection using convolutional neural network and naïve bayes data fusion," *IEEE Trans. Ind. Electron.*, vol. 65, no. 5, pp. 4392–4400, 2018.
- [3] M. Embrechts and S. Benedek, "Hybrid identification of nuclear power plant transients with artificial neural networks," *IEEE Trans. Ind. Electron.*, vol. 51, no. 3, pp. 686–693, 2004.
- [4] H. Wang, T. Chang, T. Liu, J. Huang, Z. Chen, C. Yu, R. Li, and W. Chu, "ESCM2: entire space counterfactual multi-task model for post-click conversion rate estimation," in *SIGIR*, pp. 363–372, ACM, 2022.
- [5] H. Li, W. Wang, Z. Liu, Y. Niu, H. Wang, S. Zhao, Y. Liao, W. Yang, and X. Liu, "A novel locality-sensitive hashing relational graph matching network for semantic textual similarity measurement," *Expert Systems with Applications*, vol. 207, p. 117832, 2022.
- [6] J. Fan, Y. Zhuang, Y. Liu, H. Jianye, B. Wang, J. Zhu, H. Wang, and S.-T. Xia, "Learnable behavior control: Breaking atari human world records via sample-efficient behavior selection," in *ICLR*, 2023.
- [7] Y. Huang, H. Wang, Z. Liu, L. Pan, H. Li, and X. Liu, "Modeling task relationships in multi-variate soft sensor with balanced mixture-of-experts," *IEEE Trans. Ind. Informat.*, pp. 1–9, 2022.
- [8] X. Yuan, L. Li, and Y. Wang, "Nonlinear dynamic soft sensor modeling with supervised long short-term memory network," *IEEE Trans. Ind. Informat.*, vol. 16, no. 5, pp. 3168–3176, 2019.
- [9] X. Yuan, J. Zhou, B. Huang, Y. Wang, C. Yang, and W. Gui, "Hierarchical quality-relevant feature representation for soft sensor modeling: A novel deep learning strategy," *IEEE Trans. Ind. Informat.*, vol. 16, no. 6, pp. 3721–3730, 2019.
- [10] A. Chandrakar, D. Datta, A. K. Nayak, and G. Vinod, "Statistical analysis of a time series relevant to passive systems of nuclear power plants," *Int. J. Syst. Assur. Eng. Manag.*, vol. 8, no. 1, pp. 89–108, 2017.
- [11] L. Tang, L. Yu, S. Wang, J. Li, and S. Wang, "A novel hybrid ensemble learning paradigm for nuclear energy consumption forecasting," *Appl. Energy*, vol. 93, pp. 432–443, 2012.
- [12] J. I. Aizpurua, S. D. J. McArthur, B. G. Stewart, B. Lambert, J. G. Cross, and V. M. Catterson, "Adaptive power transformer lifetime predictions through machine learning and uncertainty modeling in nuclear power plants," *IEEE Trans. Ind. Electron.*, vol. 66, no. 6, pp. 4726–4737, 2019.
- [13] H. Wang, M. Peng, R. Xu, A. Ayodeji, and H. Xia, "Remaining useful life prediction based on improved temporal convolutional network for nuclear power plant valves," *Front. Energy Res.*, vol. 8, p. 296, 2020.
- [14] Z. Wu, S. Pan, G. Long, J. Jiang, and C. Zhang, "Graph wavenet for deep spatial-temporal graph modeling," in *IJCAI*, pp. 1907–1913, 2019.
- [15] G. Lai, W.-C. Chang, Y. Yang, and H. Liu, "Modeling Long- and Short-Term Temporal Patterns with Deep Neural Networks," in *SIGIR*, pp. 95–104, 2018.
- [16] Z. Wu, S. Pan, G. Long, J. Jiang, X. Chang, and C. Zhang, "Connecting the Dots: Multivariate Time Series Forecasting with Graph Neural Networks," in *SIGKDD*, pp. 753–763, 2020.
- [17] L. Yao and Z. Ge, "Industrial big data modeling and monitoring framework for plant-wide processes," *IEEE Trans. Ind. Informat.*, vol. 17, no. 9, pp. 6399–6408, 2020.
- [18] A. Vaswani, N. Shazeer, N. Parmar, J. Uszkoreit, L. Jones, A. N. Gomez, L. Kaiser, and I. Polosukhin, "Attention is all you need," *NeurIPS*, vol. 30, 2017.
- [19] Z. Liu, Y. Lin, Y. Cao, H. Hu, Y. Wei, Z. Zhang, S. Lin, and B. Guo, "Swin transformer: Hierarchical vision transformer using shifted windows," in *Proceedings of the IEEE/CVF International Conference on Computer Vision*, pp. 10012–10022, 2021.
- [20] J. Jumper, R. Evans, A. Pritzel, T. Green, M. Figurnov, O. Ronneberger, K. Tunyasuvunakool, R. Bates, et al., "Highly accurate protein structure prediction with alphafold," *Nature*, vol. 596, no. 7873, pp. 583–589, 2021.
- [21] Y. Ma and J. Tang, *Deep Learning on Graphs*. Cambridge University Press, 2021.
- [22] Z. Chen and Z. Ge, "Directed acyclic graphs with tears," *IEEE T-AI*, 2022.
- [23] Z. Chen and Z. Ge, "Knowledge automation through graph mining, convolution and explanation framework: a soft sensor practice," *IEEE Trans. Ind. Informat.*, 2021.
- [24] Z. Wu, S. Pan, G. Long, J. Jiang, X. Chang, and C. Zhang, "Connecting the dots: Multivariate time series forecasting with graph neural networks," in *SIGKDD*, pp. 753–763, 2020.
- [25] H. Zhou, S. Zhang, J. Peng, S. Zhang, J. Li, H. Xiong, and W. Zhang, "Informer: Beyond efficient transformer for long sequence time-series forecasting," in *AAAI*, vol. 35, pp. 11106–11115, 2021.
- [26] H. C. Jung, J. Maly, L. Palzer, and A. Stollenwerk, "Quantized compressed sensing by rectified linear units," *IEEE Trans. Inf. Theory*, vol. 67, no. 6, pp. 4125–4149, 2021.
- [27] S. Wu, X. Xiao, Q. Ding, P. Zhao, Y. Wei, and J. Huang, "Adversarial sparse transformer for time series forecasting," in *NeurIPS*, vol. 33, pp. 17105–17115, 2020.
- [28] K. Champion, B. Lusch, J. N. Kutz, and S. L. Brunton, "Data-driven discovery of coordinates and governing equations," *PNAS*, vol. 116, no. 45, pp. 22445–22451, 2019.
- [29] M. Zaheer, G. Guruganesh, K. A. Dubey, J. Ainslie, C. Alberti, S. Ontañón, P. Pham, A. Ravula, Q. Wang, L. Yang, and A. Ahmed, "Big bird: Transformers for longer sequences," in *NeurIPS*, vol. 33, pp. 17283–17297, 2020.
- [30] S. L. Brunton, J. L. Proctor, and J. N. Kutz, "Discovering governing equations from data by sparse identification of nonlinear dynamical systems," *PNAS*, vol. 113, no. 15, pp. 3932–3937, 2016.
- [31] P. Ball et al., "The start-ups chasing clean, carbon-free fusion energy," *Nature*, vol. 599, no. 7885, pp. 362–366, 2021.
- [32] R. Y. Cui, N. Hultman, D. Cui, H. McJeon, S. Yu, M. R. Edwards, A. Sen, K. Song, C. Bowman, L. Clarke, et al., "A plant-by-plant strategy for high-ambition coal power phaseout in china," *Nat. Commun.*, vol. 12, no. 1, pp. 1–10, 2021.
- [33] M. B. Roth and P. Jaramillo, "Going nuclear for climate mitigation: An analysis of the cost effectiveness of preserving existing us nuclear power plants as a carbon avoidance strategy," *Energy*, vol. 131, pp. 67–77, 2017.
- [34] L. Li, A. J. Blomberg, J. D. Spengler, B. A. Coull, J. D. Schwartz, and P. Koutrakis, "Unconventional oil and gas development and ambient particle radioactivity," *Nat. Commun.*, vol. 11, no. 1, pp. 1–8, 2020.
- [35] C. Liu, W. Zhang, K. Ungar, E. Korpach, B. White, M. Benotto, and E. Pellerin, "Development of a national cosmic-ray dose monitoring system with health canada's fixed point surveillance network," *J. Environ. Radioact.*, vol. 190, pp. 31–38, 2018.
- [36] Y.-J. Huang, Z.-H. Shang-Guan, F. Zhao, M.-G. Lin, X.-D. Sha, D.-Y. Luo, Q. Chen, and K. Peng, "A correlation study of continuously monitored gamma dose rate and meteorological conditions," *J. Environ. Radioact.*, vol. 192, pp. 467–477, 2018.
- [37] J. Hirouchi, S. Hirao, J. Moriizumi, H. Yamazawa, and A. Suzuki, "Estimation of infiltration and surface run-off characteristics of radionuclides from gamma dose rate change after rain," *J. Nucl. Sci. Technol.*, vol. 51, no. 1, pp. 48–55, 2014.
- [38] J. F. Mercier, B. L. Tracy, R. D'Amours, F. Chagnon, I. Hoffman, E. P. Korpach, S. Johnson, and R. K. Ungar, "Increased environmental gamma-ray dose rate during precipitation: a strong correlation with

- contributing air mass,” *J. Environ. Radioact.*, vol. 100, no. 7, pp. 527–533, 2009.
- [39] M. Kowatari, H. Yoshitomi, S. Nishino, Y. Tanimura, T. Ohishi, P. Kessler, S. Neumaier, and A. Röttger, “Establishment of a Low Dose Rate Gamma Ray Calibration Field for Environmental Radiation Monitoring Devices,” *Radiat. Prot. Dosimetry.*, pp. 1–8, 2019.
- [40] Y. K. Chan and Y. C. Tsai, “Multiple regression approach to predict turbine-generator output for Chinshan nuclear power plant,” *Kerntechnik*, vol. 82, no. 1, pp. 24–30, 2017.
- [41] S. Grape, E. Branger, Z. Elter, and L. P. Balkeståhl, “Determination of spent nuclear fuel parameters using modelled signatures from non-destructive assay and random forest regression,” *Nucl. Instrum. Methods Phys. Res., Sect. A*, vol. 969, p. 163979, 2020.
- [42] J. Choi and S. J. Lee, “Consistency Index-Based Sensor Fault Detection System for Nuclear Power Plant Emergency Situations Using an LSTM Network,” *Sensors*, vol. 20, no. 6, p. 1651, 2020.
- [43] J. Zhang, Z. Pan, W. Bai, and X. Zhou, “Pressurizer water level reconstruction for nuclear power plant based on gru,” in *IMCCC*, pp. 1675–1679, 2018.
- [44] D. P. Kingma and J. A. Ba, “Adam: A method for stochastic optimization,” in *ICLR*, vol. 434, pp. 1–15, 2015.
- [45] T. M. Nguyen, V. Suliafu, S. J. Osher, L. Chen, and B. Wang, “Fmm-former: Efficient and flexible transformer via decomposed near-field and far-field attention,” in *NeurIPS*, vol. 34, pp. 29449–29463, 2021.